Critical behavior of active Brownian particles: Connection to field theories

Thomas Speck ⬤

Institut für Physik, Johannes Gutenberg-Universität Mainz, Staudingerweg 7-9, 55128 Mainz, Germany

We explore the relation between active Brownian particles, a minimal particle-based model for active matter, and scalar field theories. Both show a liquid-gas-like phase transition toward stable coexistence of a dense liquid with a dilute active gas that terminates in a critical point. However, a comprehensive mapping between the particle-based model parameters and the effective coefficients governing the field theories has not been established yet. We discuss conflicting recent numerical results for the critical exponents of active Brownian particles in two dimensions. Starting from the intermediate effective hydrodynamic equations, we then present a construction for a scalar order parameter for active Brownian particles that yields the active model B+. We argue that a crucial ingredient is the coupling between density and polarization in the particle current. The renormalization flow close to two dimensions exhibits a pair of perturbative fixed points that limit the attractive basin of the Wilson-Fisher fixed point, with the perspective that the critical behavior of active Brownian particles in two dimensions is governed by a strong-coupling fixed point different from Wilson-Fisher and not necessarily corresponding to Ising universality.

I. INTRODUCTION

The comprehensive understanding of critical phenomena has been one of the major successes of statistical mechanics [1], which has cumulated in the renormalization group (RG) theory and a Nobel prize for Kenneth Wilson [2]. While pushed forward by continuous transitions in equilibrium systems, critical behavior is not restricted to thermal equilibrium and many driven systems exhibit special points and phases that are governed by scale invariance [3–5]. One class of steadily driven systems, in particular, active matter comprised of many interacting units undergoing directed motion (ranging from birds to bacteria to synthetic colloidal particles) has received extensive attention lately [6–8]. Among others, the emergence of spontaneous polar order [9,10], active nematics [11], and the self-organization of chemotactic cells and bacteria [12,13] have been studied through the lens of critical phenomena and the dynamic RG [14,15].

Within the wider field of active matter, active Brownian particles (ABPs) defined through the stochastic equations of motion

$$\dot{\mathbf{r}}_k = v_0 \mathbf{e}_k + \mathbf{F}_k + \boldsymbol{\eta}_k \qquad (1)$$

have become an intensively studied paradigm for the interplay of directed motion with short-range repulsive forces $\mathbf{F}_k$ modeling volume exclusion [16]. ABPs are propelled through adding a velocity term $v_0 \mathbf{e}_k$ with fixed magnitude v_0 and *independent* unit orientations $\mathbf{e}_k$ (no alignment) that diffuse freely with orientational correlation time τ_r. The translational noise $\boldsymbol{\eta}_k$ might be absent. As first shown in simulations [17], this model undergoes *motility-induced phase separation* [18] that resembles liquid-gas phase separation in a passive fluid (or suspension) but in the absence of cohesive forces. Instead,

the blocking of particles due to the repulsive forces in combination with the persistence of forward motion leads to a dynamic instability through the dependence of the effective propulsion speed on the local density [19].

The phase diagram of monodisperse ABPs has been mapped out in simulations for several variants of the model in both two and three dimensions [20–29]. In two dimensions, the phase diagram features a coexistence region above a critical speed $\text{Pe}_c \simeq 40 \gg 1$ (in terms of the dimensionless Péclet number $\text{Pe} \equiv 3v_0\tau_r/\sigma$ with bare propulsion speed v_0, orientational correlation time τ_r, and disk diameter σ), cf. Fig. 1(a). At high densities approaching the close-packing limit, the transition of the passive fluid into a two-dimensional solid continues to nonvanishing Péclet numbers with an intermediate hexatic phase [20]. In three dimensions, qualitatively the same behavior is observed [22,23,26], although the motility-induced transition is shifted to higher Péclet numbers, indicating that in higher dimensions the blocking mechanism is less efficient, as one might expect. Very recently, it has been shown in simulations that the liquid-gas coexistence in three dimensions is in fact metastable and lies within the two-phase region of gas-solid coexistence [28,29], cf. Fig. 1(b). This is reminiscent of the phase diagram for passive colloidal suspensions with very short-range attractions [30,31]. The binodal curve of coexisting densities terminates in a critical point that has been investigated numerically in several studies, some of which claim Ising universality [32,33] as opposed to non-Ising behavior [34,35].

The coexistence of domains of low and high densities can be rationalized in field theories for a scalar order parameter field $\phi(\mathbf{r}, t)$ related to the density. Cates and coworkers extensively studied the extension of model B [36] through additional terms of schematic order ∇^4 and ϕ^2 called
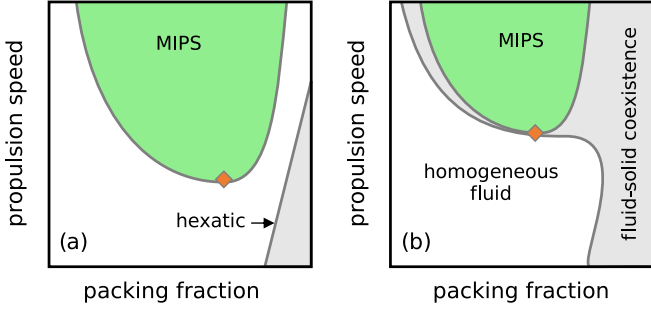
FIG. 1. Sketch of the phase diagram of monodisperse active Brownian particles in (a) two dimensions and (b) three dimensions. Indicated in green is the two-phase region within which a dense liquid domain coexists with a dilute active gas. The coexistence line ends in a critical point (diamond). Fluid-solid coexistence is indicated in light grey (with the homogeneous solid at even higher densities). In two dimensions, there is also a thin hexatic region between fluid and solid [20].

active model B+ [37–42]. These additional terms cannot be represented through a free-energy functional, in general, and potentially capture the effects of breaking detailed balance at the particle level. Since these terms are higher derivatives of the field, one would expect that they are irrelevant in the RG sense. However, an explicit one-loop calculation shows that they can induce new fixed points [41] and thus regions in model space for which the RG flow is pushed away to a nonperturbative regime. To assess this scenario for the various ABP models, one would need to explicitly calculate the coefficients of active model B+ from the microscopic model. However, such a systematic link and its verification in numerical simulations is still missing. Another line of investigation has been the mapping to an effective free energy [43,44] through the unified colored-noise approximation [45]. Such an effective action necessarily yields a ϕ^4 theory and will not be discussed in the following.

The outline of the paper is as follows: First, we review numerical results for the critical behavior of ABPs in two dimensions. We then revisit the effective hydrodynamic equations for density and polarization beyond the adiabatic approximation. We schematically expand the conditional force up to second order with four coefficients, two of which can be related to the mean-field critical point. We then derive active model B+ from these hydrodynamic equations as the nonlinear evolution of the linearly unstable mode. Building on the results for the dynamic RG of this model [41], we discuss the renormalization flow at and close to two dimensions.

II. CRITICAL BEHAVIOR

A. Background

Before we review the numerical evidence gathered so far, let us briefly recall some of the basic properties holding close to a critical point. We consider systems in d dimensions that can be described by a scalar order parameter field $\phi(\mathbf{r})$ that allows us to distinguish low density (gas) from high density

(liquid), with the average difference vanishing as a power law:

$$\langle\phi\rangle \sim (-\tau)^\beta. \qquad (2)$$

Here, τ measures the distance to the critical point and β is the corresponding critical exponent. Other quantities show a similar divergent behavior, in particular, the susceptibility

$$\int d^d\mathbf{r}' \, \langle\phi(\mathbf{r})\phi(\mathbf{r}')\rangle \sim |\tau|^{-\gamma} \qquad (3)$$

and the correlation length $\xi \sim |\tau|^{-\nu}$ defining two more critical exponents γ and ν.

In RG theory, every quantity x comes with a scaling dimension Δ_x that captures the shift $x \mapsto b^{\Delta_x}x$ under rescaling lengths $\mathbf{r} \mapsto \mathbf{r}/b$ with some factor b. Considering the correlation length $\xi \mapsto \xi/b = b^{\Delta_\xi}\xi$, we find $\Delta_\xi = -1$. Scale invariance dictates that the two-point correlation function

$$\langle\phi(\mathbf{r})\phi(\mathbf{r}')\rangle \sim \frac{1}{|\mathbf{r} - \mathbf{r}'|^{d-2+\eta}} \qquad (4)$$

decays as a power law with anomalous dimension η, which yields the scaling dimension

$$\Delta_\phi = \frac{d - 2 + \eta}{2} \qquad (5)$$

of the field. The critical exponents imply the relations $\Delta_\xi = -\nu\Delta_\tau = -1$, $\Delta_\phi = \beta\Delta_\tau = \beta/\nu$ from Eq. (2), and $d - 2\Delta_\phi = \gamma\Delta_\tau$ from Eq. (3). The latter can be rearranged to $\gamma/\nu = 2 - \eta$. We thus find the well-known hyperscaling relation

$$2\Delta_\phi + \gamma\Delta_\tau = \frac{2\beta}{\nu} + \frac{\gamma}{\nu} = d, \qquad (6)$$

restricting the exponents. Clearly, this relation is fulfilled by the Ising exponents [46]

$$\beta = \tfrac{1}{8}, \qquad \gamma = \tfrac{7}{4}, \qquad \nu = 1 \qquad (7)$$

for $d = 2$. However, note that we did not have to invoke a free energy or assume equilibriumlike behavior at any point to derive these relations.

B. Numerical results

There are now several studies, both on and off lattice, that have determined numerical values for the three critical exponents from finite-size scaling simulations, which are summarized in Fig. 2. Two lattice variants of ABPs have been studied in Ref. [35]. Variant I controls the orientational diffusion at constant speed (basically, the model of Partridge and Lee [32], who do not report independent values for β). The difference between square and hexagonal lattices is negligible. We do, however, observe a systematic shift away from the exact Ising values such that the hyperscaling relation Eq. (6) is still obeyed. Changing the dynamics (on the square lattice) to fix the rotational diffusion and change the propulsion speed leads to variant II [47], which is displaced further from Ising universality. There is an apparent violation of the hyperscaling relation, although one has to keep in mind that measuring β is challenging in these simulations and its value has the largest uncertainty. Off lattice, ABPs with fixed rotational diffusion and changing the speed v_0 have been studied in Ref. [34]. The resulting values are even further from Ising universality
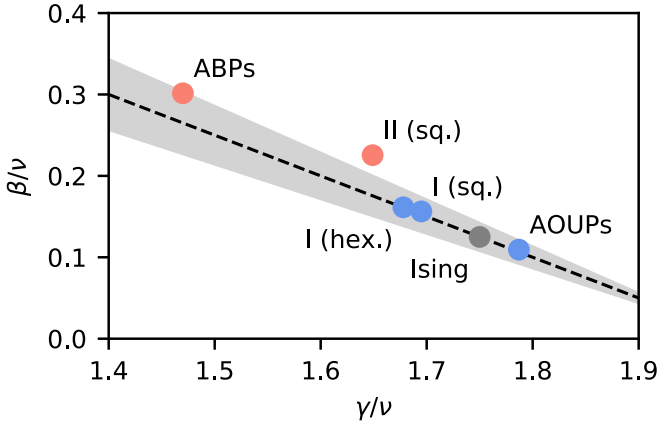
FIG. 2. Numerical estimates of critical exponents in two dimensions: off-lattice ABPs [34] and AOUPs [33], and lattice ABPs variants I (on square and hexagonal lattice) and II [35]. The dashed line is the hyperscaling relation Eq. (6) and the gray area indicates an uncertainty of $\pm 15\%$. The blue models vary the rotational diffusion time τ_r to change the Péclet number $\mathrm{Pe} \equiv 3v_0\tau_r/\sigma$ whereas the red models change the propulsion speed v_0.

but still seem to obey the hyperscaling relation within uncertainties. One explanation is that the system sizes studied are insufficient due to large corrections to scaling, which is pending further numerical investigations. Also shown are results for active Ornstein-Uhlenbeck particles (AOUPs) [48] obtained by Maggi *et al.* [33], which are related to variant I in the sense that the control parameter is the rotational diffusion but now the speed magnitude fluctuates.

III. FIELD THEORY

A. Effective hydrodynamic equations

We are interested in an effective field theory in d dimensions that describes the large-scale evolution of the slow collective degrees of freedom, typically the density. Such theories are often constructed top-down from conservation laws and symmetry considerations [49]. What we would like to achieve is to coarse grain the particle-based Eq. (1) into an evolution equation for an order parameter field. Even for passive systems, there is no unique answer. One route is to transform Eq. (1) into a stochastic field theory for a sum of δ peaks which thus contains exactly the same information [50]. Smoothing the field over some length necessarily modifies the evolution equation in a nontrivial way [51], precluding a simple correspondence between the (effective) parameters of the evolution equation and the microscopic forces. Our strategy here is based on the isotropic bulk pressure, which has been shown to predict coexisting densities of ABPs that agree very well with direct numerical estimates [52,53]. The pressure function itself needs to be determined and parametrized from computer simulations.

Our starting point is the hydrodynamic equations for ABPs that follow from the evolution of the one-body joint probability of position and orientation for a tagged particle [19,54]. Integrating out the orientation leads to a hierarchy of moments that can be closed (in the large-scale limit, viz. vanishing wave vector $q \to 0$) after the first nonconserved moment.

The zeroth moment of this hierarchy, the density $\rho(\mathbf{r}, t)$, is conserved, $\partial_t \rho + \nabla \cdot \mathbf{j} = 0$, with particle current

$$\mathbf{j} = \mathbf{p} - \ell^{-2}\nabla\rho + \mathbf{F}. \tag{8}$$

The first two terms are the current of noninteracting particles, and the conditional force $\mathbf{F}(\mathbf{r}, t)$ is a functional of the two-body correlation function taking into account the effect of surrounding particles onto a tagged particle [55]. Throughout, we employ dimensionless quantities through measuring time in units of the orientational relaxation time τ_r and lengths in units of the persistence length $v_0\tau_r$ with bare propulsion speed v_0. The control parameter thus is the scaled dimensionless persistence length $\ell \equiv v_0\sqrt{\tau_r/D_0}$ with bare translational diffusion coefficient D_0. The repulsive interactions reduce the effective propulsion speed $v(\rho)$, which becomes a function of the local density. We scale the density so the effective propulsion speed reads $v(\rho) = 1 - \rho$ and stays zero for $\rho > 1$. Such a linear decrease of the effective speed with density has been confirmed in computer simulations for ABPs [37,56].

The particle current Eq. (8) couples to the local polarization field $\mathbf{p}(\mathbf{r}, t)$, the first moment of the orientation, which obeys [19]

$$\partial_t \mathbf{p} = -\frac{1}{d}\nabla(v\rho) + \ell^{-2}\nabla^2\mathbf{p} - \mathbf{p}. \tag{9}$$

The polarization field is not conserved because of the last term, which captures the relaxation due to the free rotational diffusion. Here we have already neglected the coupling to moments of higher order, which decay even faster and are thus expected to be irrelevant in the $q \to 0$ limit. To close these hydrodynamic equations, one needs to find a representation of the conditional force $\mathbf{F}(\rho, \mathbf{p}, \nabla\rho, \dots)$ in terms of the density and polarization, and their derivatives.

B. Adiabatic mean-field theory

A simple closure is achieved through approximating the conditional force $\mathbf{F}_{\mathrm{ad}} \approx -\rho\mathbf{p}_{\mathrm{ad}}$ together with the adiabatic solution $\mathbf{p}_{\mathrm{ad}} = -\frac{1}{d}\nabla(v\rho)$ slaving the polarization to the density, which is obtained through neglecting the temporal and spatial derivatives in Eq. (9). This adiabatic solution together with the current $\mathbf{j}_{\mathrm{ad}} \approx v\mathbf{p}_{\mathrm{ad}} - \ell^{-2}\nabla\rho$ leads to a Landau mean-field theory with effective free energy [57]

$$\Psi_{\mathrm{ad}}[\phi] = \int d^d\mathbf{r}\left[\frac{1}{2}\left(\frac{1}{\ell^2} - \frac{1}{8d}\right)\phi^2 + \frac{1}{6d}\phi^4\right] \tag{10}$$

for the field $\phi = \rho - \rho_{\mathrm{c,ad}}$. A weakly nonlinear analysis around the critical point leads to the same free energy density plus a squared gradient term [57,58]. This expansion can be systematically pushed to higher orders [59,60].

While the adiabatic theory already predicts motility-induced phase separation qualitatively [57], the critical density $\rho_{\mathrm{c,ad}} = \frac{3}{4}$ and critical persistence length $\ell_{\mathrm{c,ad}} = \sqrt{8d}$ are independent of details of the microscopic interactions. A second route to the mean-field critical point is through the equation of state for the bulk pressure [53,61],

$$p(\rho; \ell) = \frac{1}{d}\rho(1 - \rho) + p_{\mathrm{IK}} + \ell^{-2}\rho, \tag{11}$$

whereby the last term is the ideal gas pressure. For a uniform fluid, the repulsive interactions between particles give rise to an isotropic pressure $p_{IK}(\rho; \ell)$ increasing monotonically with density [52,53,61], and the conditional force $\mathbf{F} = -\boldsymbol{\nabla} p_{IK}$. An interaction term of the form $p_{IK} = \ell^{-1} f(\rho)$ has been measured for active hard disks ($d = 2$) in computer simulations in the homogeneous phase ($\ell < \ell_c$) [52,53,61]. The function $f(\rho)$ captures the model-specific interactions. The two conditions for the critical point are $p'(\rho_c; \ell_c) = 0$ and $p''(\rho_c; \ell_c) = 0$ (here the prime denotes the derivative with respect to the density). For the data of Ref. [61], parametrizing the function $f(\rho)$ one finds $\rho_c \simeq 0.69$ reasonably close to 0.75 but $\ell_c \simeq 26.3$ is much larger than the adiabatic prediction $\ell_{c,ad} = 4$ in $d = 2$ [53]. The simulations of Ref. [34] find $\ell_c = Pe_c/\sqrt{3} \simeq 23$.

C. Current expansion

To improve the adiabatic result and take into account interparticle forces beyond an effective speed $v(\rho)$, we expand the conditional force in Eq. (8),

$$\mathbf{F} \approx -\ell^{-1} \boldsymbol{\nabla}[f_1 \delta\rho + f_2 (\delta\rho)^2] - \zeta \mathbf{p}\delta\rho + \zeta_p \boldsymbol{\nabla}\mathbf{p}^2, \qquad (12)$$

up to second order of polarization and density fluctuations $\delta\rho \equiv \rho - \rho_c$ away from the critical density ρ_c. The two terms inside the brackets stem from the expansion of $f(\rho)$ obtained for a uniform fluid. Even without knowledge of this function, close to the critical point we can find the coefficients from the conditions $p'(\rho_c) = 0$ and $p''(\rho_c) = 0$ at $\ell = \ell_c$, which imply $f_2 = \ell_c/d$ and $f_1 = \ell_c(\alpha - \ell_c^{-2})$. Here we have introduced the parameter $\alpha > \ell_c^{-2} > 0$, determining the critical density through $\rho_c = \frac{1}{2} + \frac{d}{2}\alpha$. The values for ℓ_c and α are determined by the functional form of $f(\rho)$ but are considered an input to the theory in the following.

The last two terms in Eq. (12) take into account the coupling between polarization and density fluctuations as well as the gradient of the polarization magnitude. The corresponding coefficients ζ and ζ_p are additional free parameters of the theory. We thus obtain the coupled hydrodynamic equations

$$\partial_t \delta\rho = c\nabla^2 \delta\rho - \boldsymbol{\nabla} \cdot \mathbf{p} + \zeta \boldsymbol{\nabla} \cdot (\mathbf{p}\delta\rho) \\ + \zeta_2 \nabla^2 (\delta\rho)^2 - \zeta_p \nabla^2 \mathbf{p}^2 \qquad (13)$$

and

$$\partial_t \mathbf{p} = \ell^{-2} \nabla^2 \mathbf{p} - \mathbf{p} + \alpha \boldsymbol{\nabla}\delta\rho + \frac{1}{d}\boldsymbol{\nabla}(\delta\rho)^2, \qquad (14)$$

with coefficients $c \equiv f_1/\ell + \ell^{-2}$ and $\zeta_2 \equiv \ell_c/(d\ell)$.

D. Linear analysis and Gaussian fixed point

We collect the density and polarization into $d + 1$ fields $p_i(\mathbf{r}, t)$, whereby $p_0 = \delta\rho$. In Fourier space,

$$p_i(\mathbf{r}, t) = \int \frac{d^d \mathbf{q} d\omega}{(2\pi)^{d+1}} e^{i(\mathbf{q}\cdot\mathbf{r} - \omega t)} p_i(\mathbf{q}, \omega), \qquad (15)$$

with magnitude $q = |\mathbf{q}|$ of the wave vector $\mathbf{q}$. The linearized hydrodynamic equations can be written $-i\omega p_i = L_{ij} p_j$, with

$(d + 1) \times (d + 1)$ matrix

$$\mathbf{L}(\mathbf{q}) = \begin{pmatrix} -cq^2 & -iq_1 & -iq_2 & \cdots \\ \alpha iq_1 & -(q/\ell)^2 - 1 & 0 & \\ \alpha iq_2 & 0 & -(q/\ell)^2 - 1 & \\ \vdots & & & \ddots \end{pmatrix}. \qquad (16)$$

We follow the summation convention and sum over repeated indices. In Appendix, we show that d eigenvalues of this matrix are of the form $-1 + O(q^2)$ and thus negative for small q, plus one eigenvalue $\sigma_+(q)$ that can be expanded for small q into $\sigma_+(q) \approx -aq^2 - \kappa q^4$ with two coefficients, the distance

$$a = c - \alpha = -(\alpha + \ell_c^{-2})(1 - \ell_c/\ell) + \ell_c^{-2}(1 - \ell_c/\ell)^2 \quad (17)$$

to the mean-field critical point and the positive stiffness:

$$\kappa = \alpha\ell_c^{-2} + \alpha(\alpha - \ell_c^{-2})(1 - \ell_c/\ell). \qquad (18)$$

For $a < 0$ ($\ell > \ell_c$), the eigenvalue σ_+ becomes positive for small q, signaling a dynamic instability.

The corresponding eigenvector $L_{ij}v_j^+ = \sigma_+ v_i^+$ reads

$$\mathbf{v}^+(q) \approx \begin{pmatrix} 1 + \frac{\kappa}{\alpha}q^2 \\ \alpha iq_1 \\ \alpha iq_2 \\ \vdots \end{pmatrix} \qquad (19)$$

up to order q^2. So far, we have ignored that the hydrodynamic equations do come with a noise term, both due to the influence of the solvent and due to the coarse graining into fields. The noise is modeled as Gaussian with zero mean and correlations:

$$\langle \eta(\hat{q})\eta(\hat{q}') \rangle = 2Dq^2(2\pi)^{d+1}\delta^d(\mathbf{q} + \mathbf{q}')\delta(\omega + \omega'). \qquad (20)$$

Note the factor q^2, which appears due to the conservation of the density. The evolution of the eigenmode $\mathbf{v}^+$ with coefficient $\phi(\mathbf{q}, \omega)$ is thus $\phi = G_0\eta$ with free propagator

$$G_0(\hat{q}) = G_0(q, \omega) \equiv \frac{1}{-i\omega + aq^2 + \kappa q^4} \qquad (21)$$

after switching to the frequency domain and writing $\hat{q} \equiv (\mathbf{q}, \omega)$. The correlation function of the eigenmode becomes

$$\langle \phi(\hat{q})\phi(\hat{q}') \rangle = (2\pi)^{d+1}C_0(\hat{q})\delta^{d+1}(\hat{q} + \hat{q}'), \qquad (22)$$

with $C_0(\hat{q}) \equiv 2Dq^2 G_0(\hat{q})G_0(-\hat{q})$. The static structure factor follows as

$$S_0(q) = \frac{1}{2\pi} \int_{-\infty}^{\infty} d\omega \, C_0(q, \omega) = \frac{D}{a + \kappa q^2}, \qquad (23)$$

from which we read off the correlation length $\xi = \sqrt{\kappa/a} \propto a^{-\nu}$ with exponent $\nu = \frac{1}{2}$. The correlation length diverges at the critical point with $S_0(q) \sim q^{-2}$. In general, $S(q) \sim q^{-2+\eta}$, and the two critical exponents $\nu = \frac{1}{2}$ and $\eta = 0$ define the Gaussian fixed point.

E. Nonlinear theory: Eigenmode expansion

We return to the evolution Eq. (13) for the density field p_0, which now reads (with index

$k = 1, \ldots, d$)

$$-i\omega p_0 = L_{0i} p_i + i\zeta q_k \int_{\hat{k}} p_k(\hat{k}) p_0(\hat{q} - \hat{k})$$

$$- \zeta_2 q^2 \int_{\hat{k}} p_0(\hat{k}) p_0(\hat{q} - \hat{k})$$

$$+ \zeta_p q^2 \int_{\hat{k}} p_k(\hat{k}) p_k(\hat{q} - \hat{k}), \qquad (24)$$

writing $\hat{k} \equiv (\mathbf{k}, \Omega)$ and

$$\int_{\hat{k}} \equiv \int \frac{d^d \mathbf{k}\, d\Omega}{(2\pi)^{d+1}}. \qquad (25)$$

Clearly, the density couples to the polarization fields p_k through the first nonlinear term. For a closure, we expand the fields into the eigenvectors of the matrix $\mathbf{L}$:

$$p_i = \sum_{n=0}^{d} \phi^{(n)} v_i^{(n)} \approx \phi v_i^+. \qquad (26)$$

In the following, we restrict our attention to the dynamics of the slowest mode amplitude $\phi(\mathbf{q}, \omega)$ corresponding to the eigenvalue $\sigma_+(q)$. Inserting $p_0 = v_0^+ \phi$ and $p_k = \alpha i q_k \phi$ into Eq. (24) yields

$$-i\omega v_0^+ \phi = \sigma_+ v_0^+ \phi - \int_{\hat{k}} [\zeta \alpha \mathbf{q} \cdot \mathbf{k} v_0^+(\mathbf{q} - \mathbf{k})$$

$$+ \zeta_2 q^2 v_0^+(k) v_0^+(\mathbf{q} - \mathbf{k})$$

$$+ \zeta_p \alpha^2 q^2 \mathbf{k} \cdot (\mathbf{q} - \mathbf{k})] \phi(\hat{k}) \phi(\hat{q} - \hat{k}). \quad (27)$$

Gathering terms into the free propagator G_0 [Eq. (21)] and including again the noise field leads to the evolution equation

$$\phi = G_0 \eta + G_0 \int_{\hat{k}} v_2(\mathbf{k}, \mathbf{q} - \mathbf{k}) \phi(\hat{k}) \phi(\hat{q} - \hat{k}), \qquad (28)$$

which is our first central result. It suggests that the scalar order parameter for the critical fluctuations is not exactly the density $\delta\rho$ but the coefficient ϕ of the slowest mode with density $\delta\rho \approx \phi - (\kappa/\alpha)\nabla^2\phi$ and polarization field $\mathbf{p} \approx \alpha\nabla\phi$ in real space. Neglecting the term $\nabla^2\phi$, we recover the linearized adiabatic solution.

In Eq. (28), we have defined the bare symmetric vertex

$$v_2(\mathbf{k}_1, \mathbf{k}_2) = \tfrac{1}{2}[v_2'(\mathbf{k}_1, \mathbf{k}_2) + v_2'(\mathbf{k}_2, \mathbf{k}_1)], \qquad (29)$$

with

$$v_2'(\mathbf{k}_1, \mathbf{k}_2) \equiv -v_0^+(k_2)[\zeta \alpha \mathbf{q} \cdot \mathbf{k}_1 + \zeta_2 q^2 v_0^+(k_1)]/v_0^+(q)$$

$$- \zeta_p \alpha^2 q^2 \mathbf{k}_1 \cdot \mathbf{k}_2 / v_0^+(q). \qquad (30)$$

Since there is only one field ϕ, $v_2(\mathbf{k}_1, \mathbf{k}_2)$ must be symmetric with respect to exchanging $\mathbf{k}_1 \leftrightarrow \mathbf{k}_2$. Note the effective momentum conservation $\mathbf{q} = \mathbf{k}_1 + \mathbf{k}_2$. In real space, this function represents a nonlocal kernel and upon expansion generates spatial derivatives of ϕ.

Let us see what these derivatives are. At the mean-field critical point with $a = 0$, we insert $v_0^+(q) \approx 1 + (q/\ell_c)^2$. To lowest order q^2, we find

$$v_2^{(2)} = -\tfrac{1}{2}\zeta\alpha\mathbf{q} \cdot (\mathbf{k}_1 + \mathbf{k}_2) - \zeta_2 q^2 = -\bar{b}q^2 \qquad (31)$$

with $\bar{b} = \zeta\alpha/2 + \zeta_2$, which corresponds to $\bar{b}\nabla^2\phi^2$ in real space. The next order comprises products of four wave vectors:

$$v_2^{(4)} = \frac{\bar{b}}{\ell_c^2} q^4 - \frac{\zeta_2}{\ell_c^2} q^2 (k_1^2 + k_2^2) - \zeta_p \alpha^2 q^2 \mathbf{k}_1 \cdot \mathbf{k}_2$$

$$- \frac{1}{2} \frac{\zeta\alpha}{\ell_c^2} (\mathbf{q} \cdot \mathbf{k}_1 k_2^2 + \mathbf{q} \cdot \mathbf{k}_2 k_1^2). \qquad (32)$$

The second term is split using $k_1^2 + k_2^2 = q^2 - 2\mathbf{k}_1 \cdot \mathbf{k}_2$ so

$$v_2^{(4)} = \frac{c_1}{2} q^4 + c_2 q^2 \mathbf{k}_1 \cdot \mathbf{k}_2 - \frac{c_3}{2}(\mathbf{q} \cdot \mathbf{k}_1 k_2^2 + \mathbf{q} \cdot \mathbf{k}_2 k_1^2), \quad (33)$$

with three further coefficients (using $\zeta_2 = 1/d$)

$$c_1 = \frac{\zeta\alpha}{\ell_c^2}, \quad c_2 = \frac{2}{d\ell_c^2} - \zeta_p \alpha^2, \quad c_3 = \frac{\zeta\alpha}{\ell_c^2}. \qquad (34)$$

In real space, these terms correspond to $\frac{1}{2}c_1 \nabla^4\phi^2$, $c_2 \nabla^2|\nabla\phi|^2$, and $-c_3 \nabla \cdot [(\nabla^2\phi)\nabla\phi]$. The values for the bare coefficients $\bar{b}$ and c_n are given to leading order at the mean-field critical point but in principle they depend on the distance a from the critical point.

The evolution Eq. (28) for the order parameter field $\phi(\mathbf{r}, t)$ in real space thus becomes

$$\partial_t \phi = \nabla^2(a\phi + \bar{b}\phi^2 - \kappa\nabla^2\phi) + \frac{c_1}{2}\nabla^4\phi^2 + c_2 \nabla^2|\nabla\phi|^2$$

$$- c_3 \nabla \cdot [(\nabla^2\phi)\nabla\phi] + \eta, \qquad (35)$$

which is precisely active model B+ and constitutes our second central result. It includes all quadratic terms involving up to four ∇'s that respect translational and rotational symmetry. Clearly, the coupling ζ between polarization and density in the conditional force [Eq. (12)] is crucial to generate the nonlinear terms with coefficients c_1 and c_3. Equation (35) corresponds to a conserved dynamical equation for ϕ with current

$$\mathbf{j}_\phi = -\nabla \frac{\delta\Psi}{\delta\phi} - \nabla\left(\frac{c_1}{2}\nabla^2\phi^2 + c_2|\nabla\phi|^2\right) + c_3(\nabla^2\phi)\nabla\phi \qquad (36)$$

involving the Landau-Ginzburg functional:

$$\Psi[\phi] \equiv \int d^d\mathbf{r} \left[\frac{\kappa}{2}|\nabla\phi|^2 + \frac{a}{2}\phi^2 + \frac{\bar{b}}{3}\phi^3 + \frac{u}{4}\phi^4\right]. \qquad (37)$$

Here we have added a ϕ^4 term with coefficient $u > 0$, which would have been generated by our expansion of $f(\rho)$ to third order [Eq. (12)] (and neglecting all other terms that would appear at this order). The cubic term $\bar{b}\phi^3$ can then be eliminated through shifting $\phi \mapsto \phi + \phi_0$ with $\phi_0 = -\bar{b}/(3u)$. This shift leads to a linear term $\propto \phi$ in Ψ which does not change the evolution equation. It also reduces $a \mapsto a - \bar{b}^2/(3u)$ with the Gaussian critical point still defined by the condition $a = 0$ as well as $\kappa \mapsto \kappa - c_1\phi_0$. Table I summarizes the fields and parameters of the coarse-grained descriptions.

IV. DISCUSSION

A. Coexistence

Before going to the critical point, let us look at state points $\ell > \ell_c$ in the two-phase region with coexisting dense and

TABLE I. Summary of the three levels of description. The only independent input to ABPs [Eq. (1)] is a pair potential $u(r)$ determining the pairwise forces. The closed hydrodynamic Eqs. (13) and (14) depend on the mean-field critical persistence length ℓ_c, α determining the mean-field critical density ρ_c, and the unknown coefficients ζ and ζ_p. Active model B+ [Eq. (35)] only involves a single scalar field $\phi(\mathbf{r}, t)$ with now seven model parameters that can be expressed through the four hydrodynamic parameters. These parameters are functions of a microscopic length Λ^{-1}.

	Degrees of freedom	Model parameters
Active model B+	$\phi(\mathbf{r}, t)$	κ, D, a, u, c_n
Effective hydrodynamics	$\rho(\mathbf{r}, t), \mathbf{p}(\mathbf{r}, t)$	$\ell_c, \alpha, \zeta, \zeta_p$
Microscopic ABPs	$\{\mathbf{r}_k, \mathbf{e}_k\}$	$u(r)$

dilute domains. First, note that the terms involving κ, c_1, and c_2 in Eq. (35) can be rewritten as

$$\nabla^2[-(\kappa - c_1\phi)\nabla^2\phi + \lambda|\nabla\phi|^2], \tag{38}$$

with $\lambda \equiv c_1 + c_2$. If we compare this expression with the functional derivative

$$\frac{\delta}{\delta\phi}\int d^d\mathbf{r}\, \frac{1}{2}\kappa(\phi)|\nabla\phi|^2 = -\kappa(\phi)\nabla^2\phi - \frac{1}{2}\kappa'(\phi)|\nabla\phi|^2, \tag{39}$$

we see that with $\kappa(\phi) \equiv \kappa - c_1\phi$ these terms can be absorbed into the Landau-Ginzburg functional Eq. (37) if the relation $\lambda = -\kappa'(\phi)/2$ holds. For the nonlinear coefficients c_n, this leads to the conditions $c_3 = 0$ and $c_1 + 2c_2 = 0$ along which a free-energy functional is restored implying equilibriumlike behavior.

Moving away from the equilibriumlike regime with $c_3 \neq 0$, Eq. (35) predicts a qualitatively new feature: droplets of the (local) minority phase have a typical finite size with smaller droplets growing and larger droplets shrinking [40]. This reverse Ostwald ripening leads to both "bubbly" phase separation with gas droplets suspended within the dense liquid as well as a state that resembles microphase separation [Fig. 3(a), see also Ref. [63] for the emergence of periodic solutions in a related type of field theory]. This process implies a distribution of droplet sizes that is peaked around the typical size as
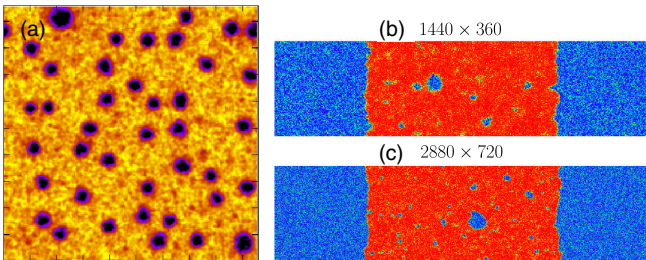

FIG. 3. Numerical results at coexistence. (a) Numerical solution of active model B+ [Eq. (35)] for $c_1 = 0$, $c_2 = 1$, and $c_3 = 4$ inside the two-phase region. (Reproduced from Ref. [40].) (b), (c) Simulation snapshots for active Brownian particles with anisotropic mobility tensor for two system sizes. (Reproduced with permission from Ref. [62].)

confirmed in numerical solutions of Eq. (35). At variance with this picture, the distribution of droplet sizes in simulations of ABPs decays algebraically and scales with the system size [62], cf. Figs. 3(b) and 3(c) (the authors even had to introduce an anisotropic mobility tensor to promote gas bubbles). Indeed, a closer looks suggests that the creation of these bubbles is connected to defects between domains of differently aligned hexatic order [64]. Moreover, it has been shown recently that the coexisting densities predicted from analytical expressions for $\kappa(\phi)$ and $\lambda(\phi)$, which have been derived from the stress, are in excellent agreement with numerical results for ABPs in $d = 2$ setting $c_3 = 0$ [53]. Together, these results suggest that the coexistence of (standard) ABPs is closer to active model B with $c_3 = 0$.

B. Perturbative renormalization

We now turn to the large-scale behavior in the vicinity of the critical point. The scaling dimension Δ_x determines whether the quantity x is relevant ($\Delta_x > 0$) or irrelevant ($\Delta_x < 0$) with the borderline $\Delta_x = 0$ termed marginal. Invariance of $a\phi + u\phi^3$ implies $\Delta_a = \Delta_u + 2\Delta_\phi$ with (naive) scaling dimension $\Delta_u = 4 - d$ so in dimensions $d > 4$ the nonlinear terms in Eq. (35) become irrelevant (they are mapped to zero under the RG flow). The critical behavior is then determined by the Gaussian critical fixed point (see Sec. III D) with a the only relevant parameter determining the distance to the Gaussian critical point. The accepted picture for the Ising model is that at $d_c = 4$, another fixed point, the Wilson-Fisher fixed point (WF), detaches from the Gaussian fixed point (G). WF moves away as d is reduced and for $d < 4$ determines the critical behavior (G now is repulsive along u while WF is attractive so any initial point not fine-tuned to $a = 0$ will flow into WF). The WF has been studied extensively through perturbative RG with good quantitative agreement with the critical exponents of the Ising model in $d = 2$ and (numerically determined) in $d = 3$ [65].

Wilson's shell renormalization scheme produces flow equations for the model parameters $\mathbf{x} = (\kappa, D, a, \dots)$ of the form

$$\partial_l x_n = (\Delta_n + \psi_n)x_n. \tag{40}$$

Here, $\psi_n(\mathbf{x})$ denotes the graphical corrections due to the recursive solution of Eq. (28), which generates a series of terms with increasing powers of the vertices. In a nutshell, internal wave vectors are integrated out in the thin shell $\Lambda/(1 + \delta l) < k < \Lambda$ with microscopic cutoff Λ leading to $\tilde{x}_n = (1 + \psi_n\delta l)x_n$. Restoring the cutoff requires us to scale external wave vectors $\mathbf{q} \to b\mathbf{q}$ with $b = 1 + \delta l$ implying $x'_n = b^{\Delta_n}\tilde{x}_n \approx (1 + \Delta_n\delta l)(1 + \psi_n\delta l)x_n$, leading to Eq. (40) in the limit $\delta l \to 0$. The model parameters $\mathbf{x}(l)$ become a function of the scale $b = e^l$. Since $\xi(l) = \xi_0 e^{-l}$, any initial values $\mathbf{x}_0$ with *finite* correlation length ξ_0 will flow to $\xi \to 0$ as $l \to \infty$. Only when hitting $\xi \to \infty$ will the flow take us to a critical fixed point of the RG flow.

Caballero *et al.* have calculated Wilson's flow equations for active model B+ including the one-loop corrections [41]. Good references for technical details of dynamic RG calculations are Refs. [15,66]. For completeness, let us recapitulate the main points. First, note that the naive scaling
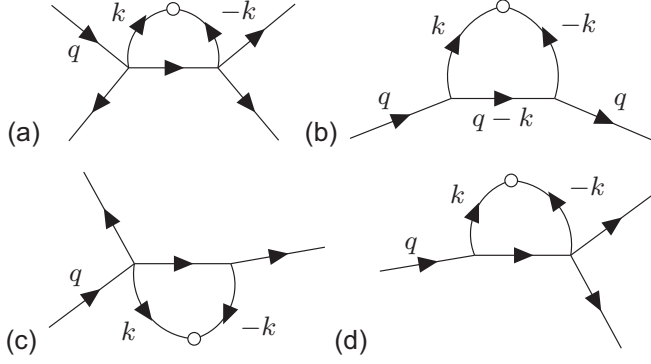
FIG. 4. Graphical representation of the relevant one-loop corrections with two vertices. Outgoing external legs represent ϕ [noise in (b)], internal lines the free propagator G_0 [Eq. (21)], and the open circle is the correlation function C_0. Each edge has an orientation and carries a wave vector (and frequency) such that at each vertex $v_n(\mathbf{k}_1, \ldots, \mathbf{k}_n)$ the sum of outgoing wave vectors $\mathbf{k}_i$ equals the single ingoing wave vector (orientations indicated by arrows).

dimensions keeping Eq. (35) invariant under rescaling length and time are $\Delta_\kappa = z - 4$, $\Delta_u = z - 2 - 2\Delta_\phi$, and $\Delta_D = \Delta_\kappa + \eta = z - 2 - d + 2\Delta_\phi$ using Eq. (5) with dynamic exponent z. Moreover, the coefficients c_n have the same scaling dimension $\Delta_c = z - 4 - \Delta_\phi$. Second, we introduce suitable reduced parameters

$$\bar{u} \equiv \frac{uD}{\kappa^2}K_d\Lambda^{4-d}, \quad \bar{c}_n \equiv \frac{c_n D^{1/2}}{\kappa^{3/2}}K_d^{1/2}\Lambda^{d/2-1} \quad (41)$$

that remove the dependence on the unknown exponents z and Δ_ϕ with $K_d \equiv S_d/(2\pi)^d$ (S_d is the surface area of a hypersphere in d dimensions).

To complement the discussion of Ref. [41] and relate to the numerical results for the critical exponents of ABPs, let us focus on the RG flow close to two dimensions through setting $d = 2 + \varepsilon$ with ε assumed to be small. To lowest order of the nonlinear coefficients u and c_n, only graphs with two vertices contribute, which are shown in Fig. 4: Fig. 4(a) is the conventional Ising contribution $\psi_u \propto u^2$, Fig. 4(b) leads to the correction $\psi_\kappa \propto c_n^2$, and Figs. 4(c) and 4(d) give rise to corrections $\psi_{c_n} \propto uc_n$. The final flow equations read

$$\partial_l \bar{u} = (2 - \varepsilon - 9\bar{u} - 2\psi_\kappa)\bar{u} \quad (42)$$

and

$$\partial_l \bar{c}_1 = \left(-\frac{\varepsilon}{2} - \frac{3}{2}\psi_\kappa\right)\bar{c}_1 - 3\bar{u}(\bar{c}_1 + 2\bar{c}_2) + \frac{9}{2}\bar{u}\bar{c}_3, \quad (43)$$

$$\partial_l \bar{c}_2 = \left(-\frac{\varepsilon}{2} - \frac{3}{2}\psi_\kappa\right)\bar{c}_2 + \frac{3}{2}\bar{u}\bar{c}_1\varepsilon - 3\bar{u}\bar{c}_3, \quad (44)$$

$$\partial_l \bar{c}_3 = \left(-\frac{\varepsilon}{2} - \frac{3}{2}\psi_\kappa\right)\bar{c}_3. \quad (45)$$

Here we have used that the noise strength D does not receive corrections ($\psi_D = 0$) and we have expanded ψ_{c_n} with the coefficients taken from Ref. [41] to leading order of ε.

For $c_n = 0$ implying $\psi_\kappa = 0$, we immediately recover the WF fixed point at $\bar{u}^* = (2 - \varepsilon)/9$. Of course, the exact value is not to be trusted close to two dimensions but it is widely accepted that the qualitative picture is correct and the WF cor-
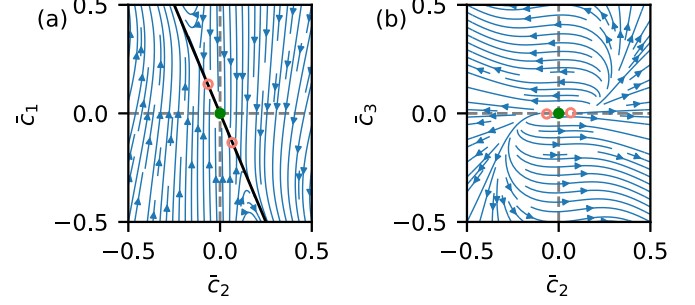

FIG. 5. Renormalization flow portrait. (a) Varying $\bar{c}_1$ and $\bar{c}_2$ for $\bar{c}_3 = 0$ and $\bar{u}^* = (2 - \varepsilon)/9$ at $\varepsilon = 0.04$. The filled symbol indicates the Wilson-Fisher fixed point and the open symbols the fixed points Eq. (47). Along the solid black line, $\bar{c}_1 + 2\bar{c}_2 = 0$ corresponding to an equilibriumlike free-energy functional. (b) Varying $\bar{c}_2$ and $\bar{c}_3$ with $\bar{c}_1 + 2\bar{c}_2 = 0$.

responds to Ising criticality even away from the upper critical dimension $d_c = 4$. For the following discussion, it is sufficient to assume that the WF sits at some positive $\bar{u}^{\mathrm{WF}} \sim O(1)$.

From Ref. [41], we find

$$\psi_\kappa = -\frac{1}{2}\bar{c}_1^2 + \bar{c}_1\bar{c}_2 - \frac{1}{4}\bar{c}_1\bar{c}_3 + \bar{c}_2^2 - 2\bar{c}_2\bar{c}_3 \quad (46)$$

at $d = 2$ (which we have confirmed independently). To determine further fixed points, we thus have to solve the set of cubic equations. The first pair is determined by $\psi_\kappa = -\varepsilon/3$, which fixes $\bar{u}^* = (2 - \varepsilon/3)/9$. The remaining equations are independent of $\bar{u}^*$ with solutions

$$\bar{c}_1^* = \pm\frac{2}{3}\varepsilon^{1/2}, \quad \bar{c}_2^* = \mp\frac{1}{3}\varepsilon^{1/2}, \quad \bar{c}_3^* = \pm\frac{1}{3}\varepsilon^{3/2} \quad (47)$$

to leading order consistent with the perturbative expansion of Eq. (35). These fixed points merge with the WF for $\varepsilon \to 0$. Moreover, they lie along the line $\bar{c}_1 + 2\bar{c}_2$ corresponding to an equilibrium-like free energy functional with stiffness $\kappa(\phi)$ discussed in the previous section IV A. Further fixed points lie outside the perturbative region. Figure 5 visualizes the flow of the nonlinear coefficients around the fixed points.

As one might expect, the scaling dimensions of the WF are not changed by the new fixed points (47). However, these fixed points strongly limit the region of the nonlinear parameters for which the WF is attractive, which vanishes entirely as $\varepsilon \to 0$. The new fixed points are attractive along the directions $\bar{u}$ and $\bar{c}_1$, and repulsive along $\bar{c}_3$. At least for small ε, the flow is attracted to the line $\bar{c}_1 + 2\bar{c}_2 = 0$ running away from the perturbative region outside the new fixed points. For $\varepsilon = 0$, the linearized flow around these fixed points reads

$$\partial_l \delta\bar{\mathbf{c}} = -3\bar{u}\begin{pmatrix} 1 & 2 & -\frac{3}{2} \\ 0 & 0 & 1 \\ 0 & 0 & 0 \end{pmatrix}\delta\bar{\mathbf{c}}, \quad (48)$$

which has eigenvector $\mathbf{e}_1 = (1, 0, 0)^T$ with eigenvalue $\Delta_1 = -3\bar{u}$ and eigenvector $\mathbf{e}_0 = (-2, 1, 0)^T$ with zero eigenvalue. Figure 5(a) shows that the flow along $\mathbf{e}_0$ is repulsive and thus marginally relevant.

V. CONCLUSIONS

As a step toward a comprehensive link between microscopic particle-based models of scalar active matter and their

continuum field theories, we have presented a route to active model B+ [Eq. (35)] starting from the intermediate hydrodynamic equations for density [Eq. (13)] and polarization [Eq. (14)]. We have identified the coupling ζ between density fluctuations and polarization in the quadratic expansion of the conditional force [Eq. (12)] as the crucial term that generates the nonpotential contributions with coefficients c_1 and c_3 to active model B+ in Eq. (35). Still missing is a strategy to calculate ζ from particle-based simulations of the microscopic equations of motion.

We have then revisited the RG flow close to two dimensions. The picture that follows from the perturbative RG in $d \to 2$ is the following: While the naive scaling dimension $\Delta_c = -\varepsilon/2$ of the nonlinear coefficients c_n indicates that they are irrelevant, they do give rise to a pair of new fixed points that destabilize the WF in two dimensions. Consequently, the parameters c_n run off to a nonperturbative regime. While one can only speculate about their fate, it is interesting to note that $\bar{c}_1$ and $\bar{c}_2$ are pulled toward values that restore the Landau-Ginzburg functional [Eq. (37)] with field-dependent stiffness $\kappa(\phi) = \kappa - c_1\phi$ and current

$$\mathbf{j}_\phi = -\nabla \frac{\delta \Psi}{\delta \phi} + c_3(\nabla^2\phi)\nabla\phi. \tag{49}$$

This suggests that two outcomes are possible: For $\zeta = 0$ implying $c_3 = 0$, one would expect indeed equilibriumlike behavior (with a strong-coupling equilibrium fixed point residing on the line $c_1 + 2c_2 = 0$). If $\zeta \neq 0$ and the coupling between density and polarization in Eq. (12) is relevant, then c_3 runs off from its initial value $c_3(0) = \zeta\alpha$ and it is conceivable that the critical behavior is governed by a non-Ising fixed point. The strong discrepancy between the numerical results for different models (Fig. 2) hints at such a possibility, in particular, between (on and off lattice) ABPs and AOUPs.

Maggi *et al.* studied the fluctuation-dissipation theorem in AOUPs in $d = 2$ dimensions as a function of wave vector q [67]. They found that the FDT is fulfilled on large length scales (small q) but violated on shorter scales. This prompted them to replace the white-noise Eq. (20) by colored noise characterized by a spatial and temporal decay scale. However, in the limit $q \to 0$ such colored noise will again reduce to

white noise and does not affect the critical properties. It does agree with our observation that the equilibrium line is attractive and, at least for AOUPs on large scales, equilibriumlike behavior obeying the fluctuation-dissipation theorem is restored. It would be interesting to study if that extends to ABPs with fixed speed magnitude, which are also characterized by the absence of persistent particle currents in the steady state. Further numerical studies are certainly welcome to shed light on the critical behavior of active particles.

APPENDIX: EIGENVALUES

We exploit that the determinant of a block matrix $\mathbf{M}$ that is decomposed into

$$\mathbf{M} = \begin{pmatrix} A & \mathbf{B} \\ \mathbf{C} & \mathbf{D} \end{pmatrix} \tag{A1}$$

reads $\det(\mathbf{M}) = (A - \mathbf{B}\mathbf{D}^{-1}\mathbf{C})\det(\mathbf{D})$. Setting $\mathbf{M} = \mathbf{L} - \sigma\mathbf{1}$ with $\mathbf{L}$ from Eq. (16), we have $A = -cq^2 - \sigma$, $\mathbf{B} = -i\mathbf{q}^T$, $\mathbf{C} = \alpha i\mathbf{q}$, and $\mathbf{D} = -(1 + (q/\ell)^2 + \sigma)\mathbf{1}$, whence the characteristic equation reads

$$\left(cq^2 + \sigma - \frac{\alpha q^2}{1 + (q/\ell)^2 + \sigma}\right)\left(1 + (q/\ell)^2 + \sigma\right)^d = 0. \tag{A2}$$

Clearly, $d - 1$ eigenvalues are given by $\sigma_0 = -1 - (q/\ell)^2$ and two more eigenvalues are the solutions $\sigma_\pm$ of a quadratic equation. We use $\mathbf{v}^\pm = (v_0^\pm, \alpha i\mathbf{q})$ as an ansatz for the eigenvector with unknown $v_0^\pm(q)$ leading to

$$\mathbf{L} \cdot \mathbf{v}^\pm = \sigma_\pm \begin{pmatrix} \frac{-cq^2 v_0^\pm + \alpha q^2}{\sigma_\pm} \\ \alpha i\mathbf{q} \end{pmatrix}, \tag{A3}$$

with $\sigma_\pm(q) = v_0^\pm(q) - 1 - (q/\ell)^2$ and $\sigma_\pm v_0^\pm = -cq^2 v_0^\pm + \alpha q^2$. The solution of these two quadratic equations yields the same $\sigma_\pm(q)$ and $v_0^+(q) \approx 1 + (\kappa/\alpha)q^2$.

[1] S.-k. Ma, *Modern Theory Of Critical Phenomena* (Routledge Taylor & Francis Group, New York, London, 2018).

[2] K. G. Wilson, The renormalization group and critical phenomena, Rev. Mod. Phys. **55**, 583 (1983).

[3] H. Hinrichsen, Non-equilibrium critical phenomena and phase transitions into absorbing states, Adv. Phys. **49**, 815 (2000).

[4] G. Ódor, Universality classes in nonequilibrium lattice systems, Rev. Mod. Phys. **76**, 663 (2004).

[5] K. Binder and P. Virnau, Phase transitions and phase coexistence: Equilibrium systems versus externally driven or active systems—Some perspectives, Soft Mater **19**, 267 (2021).

[6] C. Bechinger, R. Di Leonardo, H. Löwen, C. Reichhardt, G. Volpe, and G. Volpe, Active particles in complex and crowded environments, Rev. Mod. Phys. **88**, 045006 (2016).

[7] É. Fodor and M. Cristina Marchetti, The statistical physics of active matter: From self-catalytic colloids to living cells, Physica A **504**, 106 (2018).

[8] G. Gompper, R. G. Winkler, T. Speck, A. Solon, C. Nardini, F. Peruani, H. Löwen, R. Golestanian, U. B. Kaupp, L. Alvarez, T. Kiørboe, E. Lauga, W. C. K. Poon, A. DeSimone, S. Muiños-Landin, A. Fischer, N. A. Söker, F. Cichos, R. Kapral, P. Gaspard *et al.*, The 2020 motile active matter roadmap, J. Phys.: Condens. Matter **32**, 193001 (2020).

[9] J. Toner and Y. Tu, Long-range Order in a Two-Dimensional Dynamical XY Model: How Birds Fly Together, Phys. Rev. Lett. **75**, 4326 (1995).

[10] J. Toner and Y. Tu, Flocks, herds, and schools: A quantitative theory of flocking, Phys. Rev. E **58**, 4828 (1998).

[11] S. Mishra, R. Aditi Simha, and S. Ramaswamy, A dynamic renormalization group study of active nematics, J. Stat. Mech. (2010) P02003.

[12] A. Gelimson and R. Golestanian, Collective Dynamics of Dividing Chemotactic Cells, Phys. Rev. Lett. **114**, 028101 (2015).

[13] S. Mahdisoltani, Riccardo Ben Ali Zinati, C. Duclut, A. Gambassi, and R. Golestanian, Nonequilibrium polarity-induced chemotaxis: Emergent Galilean symmetry and exact scaling exponents, Phys. Rev. Research **3**, 013100 (2021).

[14] D. Forster, D. R. Nelson, and M. J. Stephen, Large-distance and long-time properties of a randomly stirred fluid, Phys. Rev. A **16**, 732 (1977).

[15] E. Medina, T. Hwa, M. Kardar, and Y.-C. Zhang, Burgers equation with correlated noise: Renormalization-group analysis and applications to directed polymers and interface growth, Phys. Rev. A **39**, 3053 (1989).

[16] J. Bialké, T. Speck, and H. Löwen, Active colloidal suspensions: Clustering and phase behavior, J. Non-Cryst. Solids **407**, 367 (2015).

[17] Y. Fily and M. C. Marchetti, Athermal Phase Separation of Self-Propelled Particles with no Alignment, Phys. Rev. Lett. **108**, 235702 (2012).

[18] M. E. Cates and J. Tailleur, Motility-induced phase separation, Annu. Rev. Condens. Matter Phys. **6**, 219 (2015).

[19] J. Bialké, H. Löwen, and T. Speck, Microscopic theory for the phase separation of self-propelled repulsive disks, Europhys. Lett. **103**, 30008 (2013).

[20] J. U. Klamser, S. C. Kapfer, and W. Krauth, Thermodynamic phases in two-dimensional active matter, Nat. Commun. **9**, 5045 (2018).

[21] G. S. Redner, M. F. Hagan, and A. Baskaran, Structure and Dynamics of a Phase-Separating Active Colloidal Fluid, Phys. Rev. Lett. **110**, 055701 (2013).

[22] A. Wysocki, R. G. Winkler, and G. Gompper, Cooperative motion of active Brownian spheres in three-dimensional dense suspensions, Europhys. Lett. **105**, 48004 (2014).

[23] J. Stenhammar, D. Marenduzzo, R. J. Allen, and M. E. Cates, Phase behaviour of active Brownian particles: The role of dimensionality, Soft Matter **10**, 1489 (2014).

[24] J. Bialké, J. T. Siebert, H. Löwen, and T. Speck, Negative Interfacial Tension in Phase-Separated Active Brownian Particles, Phys. Rev. Lett. **115**, 098301 (2015).

[25] D. Levis, J. Codina, and I. Pagonabarraga, Active Brownian equation of state: Metastability and phase coexistence, Soft Matter **13**, 8113 (2017).

[26] J. T. Siebert, J. Letz, T. Speck, and P. Virnau, Phase behavior of active Brownian disks, spheres, and dimers, Soft Matter **13**, 1020 (2017).

[27] P. Digregorio, D. Levis, A. Suma, L. F. Cugliandolo, G. Gonnella, and I. Pagonabarraga, Full Phase Diagram of Active Brownian Disks: From Melting to Motility-Induced Phase Separation, Phys. Rev. Lett. **121**, 098003 (2018).

[28] F. Turci and N. B. Wilding, Phase Separation and Multibody Effects in Three-Dimensional Active Brownian Particles, Phys. Rev. Lett. **126**, 038002 (2021).

[29] A. K. Omar, K. Klymko, T. GrandPre, and P. L. Geissler, Phase Diagram of Active Brownian Spheres: Crystallization and the Metastability of Motility-Induced Phase Separation, Phys. Rev. Lett. **126**, 188002 (2021).

[30] P. R. ten Wolde and D. Frenkel, Enhancement of protein crystal nucleation by critical density fluctuations, Science **277**, 1975 (1997).

[31] V. J. Anderson and H. N. W. Lekkerkerker, Insights into phase transition kinetics from colloid science, Nature (London) **416**, 811 (2002).

[32] B. Partridge and C. F. Lee, Critical Motility-Induced Phase Separation Belongs to the Ising Universality Class, Phys. Rev. Lett. **123**, 068002 (2019).

[33] C. Maggi, M. Paoluzzi, A. Crisanti, E. Zaccarelli, and N. Gnan, Universality class of the motility-induced critical point in large scale off-lattice simulations of active particles, Soft Matter **17**, 3807 (2021).

[34] J. T. Siebert, F. Dittrich, F. Schmid, K. Binder, T. Speck, and P. Virnau, Critical behavior of active Brownian particles, Phys. Rev. E **98**, 030601(R) (2018).

[35] F. Dittrich, T. Speck, and P. Virnau, Critical behavior in active lattice models of motility-induced phase separation, Eur. Phys. J. E **44**, 53 (2021).

[36] P. C. Hohenberg and B. I. Halperin, Theory of dynamic critical phenomena, Rev. Mod. Phys. **49**, 435 (1977).

[37] J. Stenhammar, A. Tiribocchi, R. J. Allen, D. Marenduzzo, and M. E. Cates, Continuum Theory of Phase Separation Kinetics for Active Brownian Particles, Phys. Rev. Lett. **111**, 145702 (2013).

[38] R. Wittkowski, A. Tiribocchi, J. Stenhammar, R. J. Allen, D. Marenduzzo, and M. E. Cates, Scalar $\Phi4$ field theory for active-particle phase separation, Nat. Commun. **5**, 4351 (2014).

[39] C. Nardini, É. Fodor, E. Tjhung, F. van Wijland, J. Tailleur, and M. E. Cates, Entropy Production in Field Theories without Time-Reversal Symmetry: Quantifying the Non-Equilibrium Character of Active Matter, Phys. Rev. X **7**, 021007 (2017).

[40] E. Tjhung, C. Nardini, and M. E. Cates, Cluster Phases and Bubbly Phase Separation in Active Fluids: Reversal of the Ostwald Process, Phys. Rev. X **8**, 031080 (2018).

[41] F. Caballero, C. Nardini, and M. E. Cates, From bulk to microphase separation in scalar active matter: A perturbative renormalization group analysis, J. Stat. Mech. (2018) 123208.

[42] M. E. Cates, Active field theories, arXiv:1904.01330.

[43] M. Paoluzzi, C. Maggi, U. Marini Bettolo Marconi, and N. Gnan, Critical phenomena in active matter, Phys. Rev. E **94**, 052602 (2016).

[44] M. Paoluzzi, C. Maggi, and A. Crisanti, Statistical field theory and effective action method for scalar active matter, Phys. Rev. Research **2**, 023207 (2020).

[45] P. Jung and P. Hänggi, Dynamical systems: A unified colored-noise approximation, Phys. Rev. A **35**, 4464 (1987).

[46] L. Onsager, Crystal statistics. I. A two-dimensional model with an order-disorder transition, Phys. Rev. **65**, 117 (1944).

[47] S. Whitelam, K. Klymko, and D. Mandal, Phase separation and large deviations of lattice active matter, J. Chem. Phys. **148**, 154902 (2018).

[48] D. Martin, J. O'Byrne, M. E. Cates, É. Fodor, C. Nardini, J. Tailleur, and F. van Wijland, Statistical mechanics of active Ornstein-Uhlenbeck particles, Phys. Rev. E **103**, 032607 (2021).

[49] H. Spohn, Kinetic equations from Hamiltonian dynamics: Markovian limits, Rev. Mod. Phys. **52**, 569 (1980).

[50] D. S. Dean, Langevin equation for the density of a system of interacting Langevin processes, J. Phys. A: Math. Gen. **29**, L613 (1996).

[51] A. J. Archer and M. Rauscher, Dynamical density functional theory for interacting Brownian particles: Stochastic or deterministic? J. Phys. A: Math. Gen. **37**, 9325 (2004).

[52] A. P. Solon, J. Stenhammar, M. E. Cates, Y. Kafri, and J. Tailleur, Generalized thermodynamics of motility-induced phase separation: Phase equilibria, Laplace pressure, and change of ensembles, New J. Phys. **20**, 075001 (2018).

[53] T. Speck, Coexistence of active Brownian disks: Van der Waals theory and analytical results, Phys. Rev. E **103**, 012607 (2021).

[54] S. Steffenoni, G. Falasco, and K. Kroy, Microscopic derivation of the hydrodynamics of active-Brownian-particle suspensions, Phys. Rev. E **95**, 052142 (2017).

[55] T. Speck, Collective forces in scalar active matter, Soft Matter **16**, 2652 (2020).

[56] A. Fischer, A. Chatterjee, and T. Speck, Aggregation and sedimentation of active Brownian particles at constant affinity, J. Chem. Phys. **150**, 064910 (2019).

[57] T. Speck, A. M. Menzel, J. Bialké, and H. Löwen, Dynamical mean-field theory and weakly non-linear analysis for the phase separation of active Brownian particles, J. Chem. Phys. **142**, 224109 (2015).

[58] T. Speck, J. Bialké, A. M. Menzel, and H. Löwen, Effective Cahn-Hilliard Equation for the Phase Separation of Active Brownian Particles, Phys. Rev. Lett. **112**, 218304 (2014).

[59] L. Rapp, F. Bergmann, and W. Zimmermann, Systematic extension of the Cahn-Hilliard model for motility-induced phase separation, Eur. Phys. J. E **42**, 57 (2019).

[60] J. Bickmann and R. Wittkowski, Predictive local field theory for interacting active Brownian spheres in two spatial dimensions, J. Phys.: Condens. Matter **32**, 214001 (2020).

[61] A. P. Solon, J. Stenhammar, R. Wittkowski, M. Kardar, Y. Kafri, M. E. Cates, and J. Tailleur, Pressure and Phase Equilibria in Interacting Active Brownian Spheres, Phys. Rev. Lett. **114**, 198301 (2015).

[62] X.-q. Shi, G. Fausti, H. Chaté, C. Nardini, and A. Solon, Self-Organized Critical Coexistence Phase in Repulsive Active Particles, Phys. Rev. Lett. **125**, 168001 (2020).

[63] F. J. Thomsen, L. Rapp, F. Bergmann, and W. Zimmermann, Periodic patterns displace active phase separation, New J. Phys. **23**, 042002 (2021).

[64] C. B. Caporusso, P. Digregorio, D. Levis, L. F. Cugliandolo, and G. Gonnella, Motility-Induced Microphase and Macrophase Separation in a Two-Dimensional Active Brownian Particle System, Phys. Rev. Lett. **125**, 178004 (2020).

[65] J. Le Guillou and J. Zinn-Justin, Accurate critical exponents from the ϵ-expansion, J. Phys. Lett. **46**, 137 (1985).

[66] U. C. Täuber, Renormalization group: Applications in statistical physics, Nucl. Phys. B, Proc. Suppl. **228**, 7 (2012).

[67] C. Maggi, N. Gnan, M. Paoluzzi, E. Zaccarelli, and A. Crisanti, Critical active dynamics is captured by a colored-noise driven field theory, Commun. Phys. **5**, 55 (2022).